Metal-insulator transition in 8 − *Pmmn* borophene under normal incidence of electromagnetic radiation

Abdiel E. Champo
Facultad de Ciencias en Física y Matemáticas, Universidad Autónoma de Chiapas, Carretera Emiliano Zapata, Km. 8, Rancho San Francisco, 29050, Tuxtla Gutiérrez, Chiapas, México

Gerardo G. Naumis*
Departamento de Sistemas Complejos, Instituto de Fisica, Universidad Nacional Autónoma de México, Apartado Postal 20-364, 01000, Ciudad de México, México

(Received 13 September 2018; published 9 January 2019)

The energy spectrum for the problem of 8 − *Pmmn* borophene's electronic carriers under normal incidence of electromagnetic waves is studied without the use of any perturbative technique. This allows us to study the effects of very strong fields. To obtain the spectrum and wave functions, the time-dependent Dirac equation is solved by using a frame moving with the space-time cone of the wave, i.e., by transforming the equation into an ordinary differential equation in terms of the wave phase, leading to an electron-wave quasiparticle. The limiting case of strong fields is thus analyzed. The resulting eigenfunctions obey a generalized Mathieu equation, i.e., of a classical parametric pendulum. The energy spectrum presents bands and a gap at the Fermi energy. The gaps are due to the space-time diffraction of electrons in phase with the electromagnetic field, i.e., electrons in borophene acquire an effective mass under strong electromagnetic radiation.

DOI: 10.1103/PhysRevB.99.035415

I. INTRODUCTION

In recent times, Dirac materials have attracted intense research interest after the most celebrated discovery of an atomically two-dimensional (2D) hexagonal carbon allotrope, graphene [1], owing to its peculiar band structure and applications in the next generation of nanoelectronics [2–4].

Following the seminal discovery of graphene, great efforts have been paid to search for new Dirac materials which can host massless Dirac fermions (MDF) [5,6], especially in monolayer structures.

Recently, there has been intense research interest in the synthesis of 2D crystalline boron structures, referred to as borophenes. See as an example of the structure shown in Fig. 1. Boron is a fascinating element due to its chemical and structural complexity, and boron- based nanomaterials of various dimensions have attracted a lot of attention [7]. For example, two-dimensional phases of boron with space groups *Pmmm* and *Pmmn* and hosting MDF were theoretically predicted [8]. Several attempts have been made to synthesize a stable structure of borophene, but only three different quasi-2D structures of borophene have been synthesized [9]. Various numerical experiments have predicted a large number of borophene structures with various geometries and symmetries [8,10]. The orthorhombic 8 − *Pmmn* borophene is one of the energetically stable structures, having ground-state energy lower that of the α-sheet structures and its analogues. The *Pmmn* boron structures have two nonequivalent sublattices. The coupling and buckling between two sublattices and vacancy give rise to energetic stability as well as tilted anisotropic Dirac cones [11]. The coupling between different sublattices enhances the strength of the boron-boron bonds and hence gives rise to structural stability. The finite thickness is required for energetic stability of 2D boron allotropes. The orthorombic 8 − *Pmmn* borophene possesses tilted anisotropic Dirac cones and is a zero-gap semiconductor. It can be thought of as topologically equivalent to the distorted graphene.

A tight binding-model of 8 − *Pmmn* borophene has been recently developed [12,13] and an effective low-energy Hamiltonian in the vicinity of Dirac points was proposed on symmetry consideration. Pseudomagnetic fields were also predicted similar to those in strained graphene [4,14–17] and its relationship with electronic [18,19] and optical conductivity [20,21].

In 8 − *Pmmn* borophene, the effective low-energy Hamiltonian was used to study the plasmon dispersion and screening properties by calculating the density- density response function [22,23], the optical conductivity [24], Weiss oscillations [25], and oblique Klein tunneling [26]. The fast-growing experimental confirmation of various borophene monolayers make 8 − *Pmmn* borophene promising. However, the calculated properties of electrons under electromagnetic fields are all based on perturbative approaches. Yet, it is known that in graphene, interesting nonlinear effects appear when strong fields are applied [27–29].

In fact, a modern quantum optics approach requires the electron + strong electromagnetic field system to be treated as a whole [27,29]. Thus the light-induced renormalization of the electronic properties of Dirac materials are the subject of intense studies. As examples, we can cite the energy gap

*naumis@fisica.unam.mx

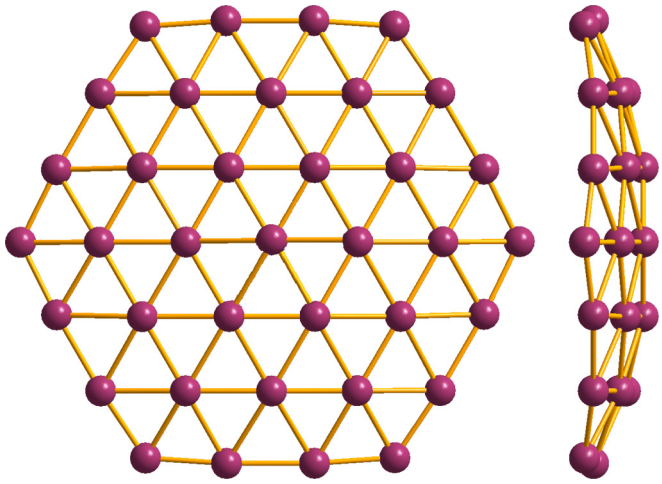

FIG. 1. Borophene lattice for the crystal phase with space group $8-Pmmn$.

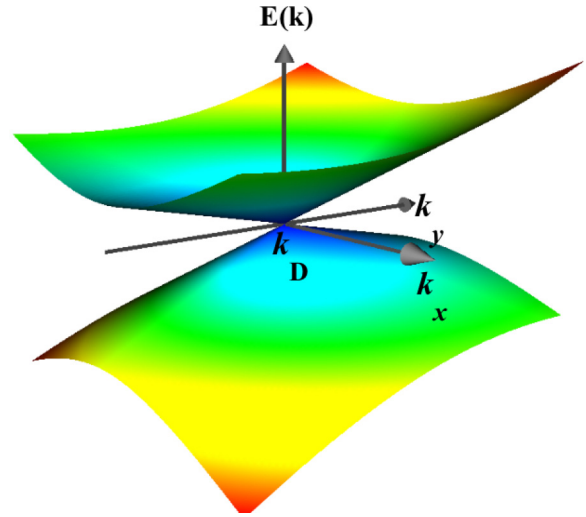

FIG. 2. Plot of the energy dispersion $E(\mathbf{k})$ as a function of $\mathbf{k}$ [see Eq. (2)] in the region around a Dirac cone. Notice the tilted anisotropy of the Dirac cone.

opening in graphene [27], the renormalization of the electron energy spectrum near the Dirac point of graphene by a strong off-resonant electromagnetic field (dressing field), and its dependence on the field polarization [29–31]. Such dressing fields can serve as an effective tool to control valley properties of the materials and be potentially exploited in optoelectronic applications [27,29–31]. Other works considered the optical response [32], transport in graphene-based p-n junctions [33], and through-dressed edge states in graphene [34–36]. More recently, interesting complex topological-phase diagrams produced by dressing fields in graphene have been found [37–40].

In this paper, we solve the problem of borophene's electron behavior in the presence of a strong electromagnetic plane wave. As a result, we are able to find the spectrum, wave functions, and a dynamic gap opening. This is like if electron in borophene acquires an effective mass under electromagnetic radiation. It is important to remark that strain affects the optoelectronics properties of 2D materials, such as phosphorene [41] or graphene [4], and these effects can be also studied by using the present methodology, as strain and flexural waves can be considered as pseudoelectromagnetic waves [15,42].

The paper is organized as follows. In Sec. II, we introduce the low-energy effective Hamiltonian and obtain the Hill's equation that solves the problem of borophene's electron behavior under electromagnetic radiation without the need of any approximation. Section III is devoted to solve the Mathieu's equation with the strong electromagnetic field approximation or long wavelength and we obtain as the solution the Mathieu cosine and Mathieu sine functions; besides, we study the stability chart of the solutions. Finally, we summarize and conclude in Sec. IV.

II. MODEL HAMILTONIAN

We start with the single-particle low-energy effective model Hamiltonian of the tilted anisotropic Dirac cones as [13]

$$\hat{H} = \varrho(v_x \hat{P}_x \sigma_x + v_y \hat{P}_y \sigma_y + v_t \hat{P}_y \sigma_0), \tag{1}$$

where the first two terms correspond to the kinetic energy term and the last term described the tilted nature of Dirac cones. The two Dirac points $\mathbf{k} = \pm\mathbf{k_D}$ are described by the valley index $\varrho = \pm 1$. The three velocities along each coordinate are given by $\{v_x, v_y, v_t\} = \{0.86, 0.69, 0.32\}$ in units of $v_F = 10^6$ m/s. The velocity v_t arises due to the tilting of the Dirac cones. Also, (σ_x, σ_y) are the Pauli matrices and σ_0 is the identity matrix. $\hat{P}_x$, $\hat{P}_y$ are the electron momentum operators. The energy dispersion of the above Hamiltonian can be readily obtained as [25]

$$E^{\varrho}_{\lambda,k} = \varrho\hbar v_t k_y + \lambda\hbar\sqrt{v_x^2 k_x^2 + v_y^2 k_y^2} \tag{2}$$

and

$$\psi^{\varrho}_{\lambda,\mathbf{k}} = \varrho\frac{e^{i\mathbf{k}\cdot\mathbf{r}}}{\sqrt{2}}\begin{pmatrix} 1 \\ \lambda e^{i\Theta} \end{pmatrix}, \tag{3}$$

where $\lambda = \pm 1$ is the band index, $\Theta = \tan^{-1}(v_y k_y / v_x k_x)$, and the $2D$ momentum vector is given by $\boldsymbol{k} = (k_x, k_y)$. The energy dispersion for the K valley is shown in Fig. 2.

A. Inclusion of electromagnetic field

For borophene irradiated by a propagating electromagnetic field perpendicular to the graphene plane, the Dirac Hamiltonian can be obtained by using the minimal coupling,

$$\hat{H} = \begin{pmatrix} v_t \hat{\Pi}_y & v_x \hat{\Pi}_x - i v_y \hat{\Pi}_y \\ v_x \hat{\Pi}_x + i v_y \hat{\Pi}_y & v_t \hat{\Pi}_y \end{pmatrix}, \tag{4}$$

where $\hat{\Pi} = \hat{P} - (e/c)\mathbf{A}$ and $\mathbf{A}$ is the vector potential of the applied electromagnetic field, given by $\mathbf{A} = \frac{E_0}{\Omega}\cos(Gz - \Omega t)(\cos(\theta), \sin(\theta))$, where Ω is the frequency of the wave and E_0 is the amplitude of the electric field, taken as a constant, and z is the height above the borophene's plane. The dynamics of charge carriers in graphene is governed by a time-dependent Dirac equation:

$$\hat{H}(x, y, t)\boldsymbol{\Psi}(x, y, t) = i\hbar\frac{\partial}{\partial t}\boldsymbol{\Psi}(x, y, t), \tag{5}$$

where

$$\mathbf{\Psi}(x, y, t) = \begin{pmatrix} \Psi_A(x, y, t) \\ \Psi_B(x, y, t) \end{pmatrix} \tag{6}$$

is a two-component spinor which give the electron's wave function on each borophene sublattice, denoted by A and B. To find the eigenstates and eigenenergies we use instead Pauli matrices and spinors. First, we write the equations of motion for each component of the spinor:

$$i\hbar \frac{\partial \Psi_A(x, y, t)}{\partial t} = (v_x \hat{\Pi}_x - i v_y \hat{\Pi}_y)\Psi_B(x, y, t) + v_t \hat{\Pi}_y \Psi_A(x, y, t), \tag{7}$$

$$i\hbar \frac{\partial \Psi_B(x, y, t)}{\partial t} = (v_x \hat{\Pi}_x - i v_y \hat{\Pi}_y)\Psi_A(x, y, t) + v_t \hat{\Pi}_y \Psi_B(x, y, t). \tag{8}$$

The most important step in the solution of this problem is to propose a solution of the form

$$\Psi_\rho(x, y, t) = e^{i(\mathbf{k}\cdot\mathbf{r} - Et/\hbar)}\Phi_\rho(\phi), \tag{9}$$

where we have defined the phase ϕ of the electromagnetic wave as $\phi = Gz - \Omega t$, evaluated at $z = 0$, and $\Phi_\rho(\phi)$ is a function to be determined for $\rho = A, B$. This ansatz is equivalent to consider the problem in the space-time frame of the moving wave. As detailed in the Appendix A, the system of differential equations can be further rewritten in terms of two new functions $\Gamma_A(\phi)$ and $\Gamma_B(\phi)$, defined by

$$\Gamma_\rho(\phi) = \exp\left\{-\frac{i}{c}[(v_t\tilde{k}_y - v_y\tilde{E})\phi - v_t\tilde{\xi}\sin\phi\sin\theta]\right\}\Phi_\rho(\phi), \tag{10}$$

and obtain

$$\frac{d\Gamma_A(\phi)}{d\phi} = iC^*(\phi)\Gamma_B(\phi), \tag{11}$$

$$\frac{d\Gamma_B(\phi)}{d\phi} = iC(\phi)\Gamma_A(\phi), \tag{12}$$

where

$$C(\phi) = \frac{[v_x(\tilde{k}_x - \tilde{\xi}\cos\phi\cos\theta) + i v_y(\tilde{k}_y - \tilde{\xi}\cos\phi\sin\theta)]}{c} \tag{13}$$

and the other are adimensional variables, defined as $\tilde{E} = E/(\hbar v_y G)$, $\tilde{\mathbf{k}} = \mathbf{k}/G$, $\tilde{\xi} = eE_o/(c\hbar G\Omega)$. Finally, $c = \Omega/G$ is the light velocity.

As explained in the Appendix A, Eqs. (11) and (12) can be written as a single second-order ordinary differential equation. In the resulting equation, we consider the transformation:

$$\Gamma_A(\phi) = e^{-i(\beta/2)}\chi_A(\phi), \tag{14}$$

$$\Gamma_B(\phi) = e^{i(\beta/2)}\chi_B(\phi), \tag{15}$$

where $\beta = \arctan((v_y/v_x)\tan\theta)$; besides, if we consider that

$$\chi(\phi) = \begin{pmatrix} \chi_A(\phi) \\ \chi_B(\phi) \end{pmatrix}, \tag{16}$$

we finally obtain that the $\chi(\phi)$ functions follow a Hill's equation,

$$\frac{d^2}{d\phi^2}\chi(\phi) + F(\phi)\chi(\phi) = 0, \tag{17}$$

with $F(\phi)$ defined as

$$F(\phi) = \left(\frac{1}{\hbar\Omega}\right)^2\left[\zeta^2\cos^2\phi - 2\zeta\frac{\vec{\nu}\cdot\vec{\kappa}}{|\vec{\nu}|}\cos\phi\right] + \left(\frac{\epsilon}{\hbar\Omega}\right)^2 - i\frac{\zeta}{\hbar\Omega}\sigma_x\sin\phi, \tag{18}$$

where $\epsilon = \hbar\sqrt{(v_x k_x)^2 + (v_y k_y)^2}$, $\vec{\kappa} = \hbar(v_x k_x, v_y k_y)$,
$\zeta = (eE_0/c\Omega)\sqrt{v_x^2\cos^2\theta + v_y^2\sin^2\theta}$, and
$\vec{\nu} = (v_x\cos\theta, v_y\sin\theta)$.

III. SPECTRUM AND EIGENFUNCTIONS

The resulting Hill equation, given by expression Eq. (17), is difficult to be solved analytically for all cases. Yet, the most interesting case for the physics of the problem is the limit of intense applied electric fields or long wavelengths ($E_0/\hbar\Omega^2 >> 300$), since other limits can be tackled using perturbative approaches.

For this particular case $\zeta/\hbar\Omega >> 1$, and thus in Eq. (17), we can neglect linear terms in $\zeta/\hbar\Omega$. Also, in what follows we take $\vec{\nu}\cdot\vec{\kappa} = 0$, which is basically an initial condition, to simplify the equations, although the general case can be solved in a similar way. The following equation is obtained for $\chi(\phi)$:

$$\chi''(\phi) + \left\{\frac{\epsilon^2}{(\hbar\Omega)^2} + \left(\frac{\zeta\cos\phi}{\hbar\Omega}\right)^2\right\}\chi(\phi) = 0. \tag{19}$$

Using the relation $\cos^2(\phi) = \frac{1}{2}(1 + \cos(2\phi))$, we can write

$$\chi''(\phi) + \left\{\left(\frac{\epsilon}{\hbar\Omega}\right)^2 + \left(\frac{\zeta}{\hbar\Omega}\right)^2\left[\frac{1}{2}(1 + \cos(2\phi))\right]\right\}\chi(\phi) = 0, \tag{20}$$

and defining

$$q = -\left(\frac{\zeta}{2\hbar\Omega}\right)^2 \tag{21}$$

and

$$a = \left(\frac{\epsilon}{\hbar\Omega}\right)^2 - 2q. \tag{22}$$

Thus, Eq. (19) is transformed into the following Mathieu equation:

$$\frac{d^2}{d\phi^2}\chi(\phi) + [a - 2q\cos(2\phi)]\chi(\phi) = 0. \tag{23}$$

As is well known, this Mathieu equation describes a parametric pendulum in which there is an interplay between two frequencies; one is the fundamental of the pendulum, determined by $\sqrt{a}$, and the other is the frequency of the cosine driving. The parameter q measures the coupling between the natural and driving frequencies leading to an interesting resonance phase-diagram.

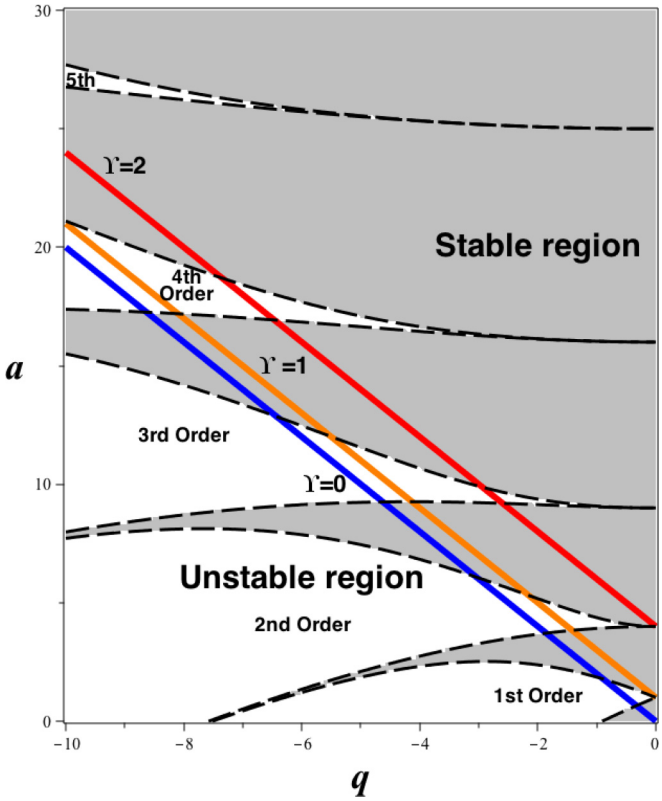

FIG. 3. Stability chart as a function of the nondimensional parameters a and q for Mathieu solutions. The regions of stability (gray domains) and instability (white domains) are divided by the characteristic curves $a_n(q)$ and $b_n(q)$ (dashed lines). This spectrum is for the case of intense electric fields or long wavelengths. In this case, there is a constraint due to Eq. (22). For fixed energies ϵ, this condition is equivalent to draw a set of parallel lines as shown in the figure, where $\Upsilon = \epsilon/\hbar\Omega$. The line $a = -2q$, i.e., $\Upsilon = 0$, divides the spectrum into two zones, the zone on the left side of this line is strictly not allowed, while the values on the right side are allowed. A simple analysis of this figure reveals bands separated by energy gaps. The order of the gaps is indicated.

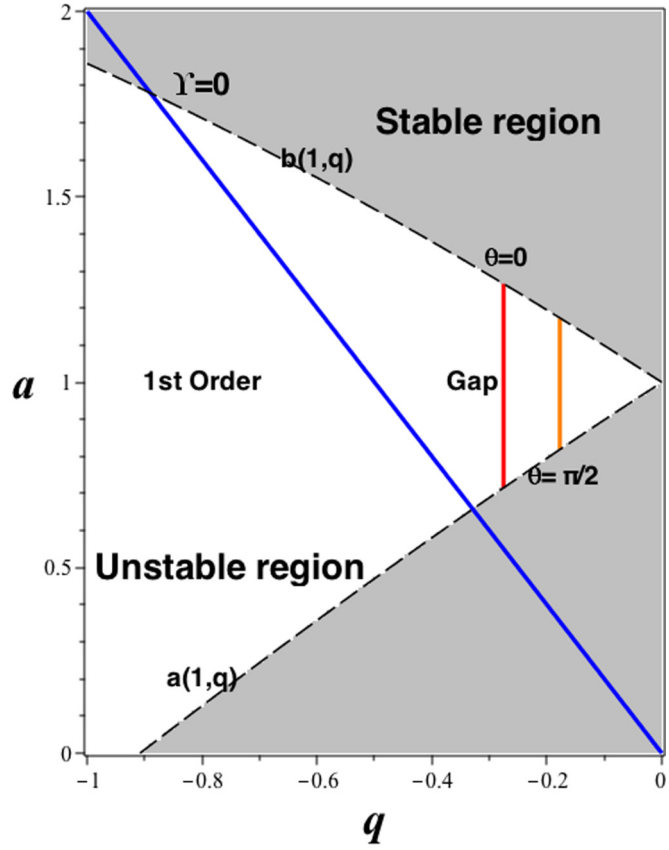

FIG. 4. Amplification of the energy spectrum for the case of long wave length near of $\Upsilon = 0$, i.e., $\epsilon = 0$. For a fixed field ($E_0 = 2$ V/m), the figure shows two energy first-order gaps for $\theta = 0$ and $\theta = \pi/2$, respectively, and two energy bands. We observe that the gap size decrease while θ increase for $0 \leqslant \theta \leqslant \pi/2$.

In our problem, the general solutions to the components χ_A y χ_B are linear combinations of the Mathieu cosine $\mathcal{C}(a, q, \phi)$ and Mathieu sine $\mathcal{S}(a, q, \phi)$ functions. Nevertheless, taking into account that when the electromagnetic field is switched out, the wave function Ψ must reduce to a free-particle wave function, we obtain that

$$\Psi(x, y, t) = N\, e^{i(\boldsymbol{k}\cdot\boldsymbol{r} - Et/\hbar - \beta/2)}\, e^{\frac{i}{c}\left[(v_t\tilde{k}_y - v_y\tilde{E})\phi - v_t\tilde{\xi}\sin\phi\sin\theta\right]} \times (\mathcal{C}(a, q, \phi) + i\mathcal{S}(a, q, \phi))\begin{pmatrix} 1 \\ \lambda e^{i(\beta+\Theta)} \end{pmatrix}, \tag{24}$$

where $\beta = \tan^{-1}[(v_y/v_x)\tan\theta]$, $\Theta = \tan^{-1}(v_y k_y/v_x k_x)$, N is a normalization constant, and $\lambda = \pm 1$ denotes the conduction and valence bands, respectively.

As it is well documented [43], the stability of Mathieu functions depends on the parameters a and q. In Fig. 3, the white regions in the (a, q) plane are those for which the solutions are unstable and therefore, are not acceptable. On the other hand, the gray regions are those for which the solutions are acceptable wave functions. The boundaries between these regions are determined by the eigenvalues, $a_n(q)$ and $b_n(q)$, corresponding to the 2π- periodic Mathieu functions of integer order, $ce_n(q, \phi)$ and $se_n(q, \phi)$, respectively [43]. As a consequence of the Mathieu solutions mentioned above, a band structure naturally emerges in our problem. However, in the present case there is an extra constraint that relates a and q due to Eq. (22). For fixed energies ϵ, this condition is equivalent to drawing a set of parallel lines in Fig. 3. Since Υ^2, where $\Upsilon = (\epsilon/\hbar\Omega)$, is always positive, in Fig. 3 we plot the line $a = -2q$, which divides the spectrum into two zones. Energies on the left side of this line are strictly not allowed, while the values on the right side are allowed. States over this line have $\Upsilon = 0$. Notice that for a fixed electric field and an angle θ, q is constant. Using this method, a simple analysis of Fig. 3 reveals bands separated by energy gaps. The opening of these gaps is due to the space-time diffraction of electrons in phase with the electromagnetic field, and effect akin to the magnetoacoustic diffraction of electrons in phase with acoustic waves [44,45]. One can think as if electrons in borophene acquire an effective mass under electromagnetic radiation, leading to a metal-insulator transition. This effect also occurs in graphene [27,28,30].

Since this approach is for intense electric fields, let us estimate the size of these gaps. For a typical microwave

frequency $\Omega = 50$ GHz with an intensity $E_0 = 2\ V/m$ of the electric field, in Appendix B we show that the first-order gap size is $\Delta \approx 0.024 \times 10^{-3}$ eV for $\theta = 0$.

IV. CONCLUSIONS

In conclusion, we have found an equation that describes the interaction between carriers in borophene under electromagnetic radiation. By solving this equation, we found the energy spectrum for intense electric field (or long wavelength). The main features of the spectra are that bands appear and are separated by energy gaps; besides, the angle θ is important for the gap size. Thus, there is a metal-insulator transition and the conductivity can be controlled by applying an electromagnetic wave. Furthermore, our analysis reveals that electrons in borophene acquire an effective mass. This is due to the diffraction of electrons in phase with the electromagnetic wave, as happens in magnetoacoustic effects in metals [45].

ACKNOWLEDGMENTS

We thank DGAPA-PAPIIT Project No. IN-102717 for financial support. A.E.C. thanks Instituto de Física for hospitality during a visit to finish this work.

APPENDIX A

In this Appendix, we derive Eqs. (11), (12), and (17). We start from Eqns. (7), (8), and (9), which are explicitly given by

$$\frac{d\Phi_A(\phi)}{d\phi} = \frac{i}{c}\{[v_t(\tilde{k}_y - \tilde{\xi}\cos\phi\sin\theta) - v_y\tilde{E}]\Phi_A(\phi) + [v_x(\tilde{k}_x - \tilde{\xi}\cos\phi\cos\theta) - iv_y(\tilde{k}_y - \tilde{\xi}\cos\phi\sin\theta)]\Phi_B(\phi)\}, \tag{A1}$$

$$\frac{d\Phi_B(\phi)}{d\phi} = \frac{i}{c}\{[v_t(\tilde{k}_y - \tilde{\xi}\cos\phi\sin\theta) - v_y\tilde{E}]\Phi_B(\phi) + [v_x(\tilde{k}_x - \tilde{\xi}\cos\phi\cos\theta) + iv_y(\tilde{k}_y - \tilde{\xi}\cos\phi\sin\theta)]\Phi_A(\phi)\}, \tag{A2}$$

where $\tilde{E} = \frac{E}{\hbar v_y G}$, $\tilde{\mathbf{k}} = \frac{1}{G}\mathbf{k}$, $\tilde{\xi} = \frac{eE_o}{c\hbar G\Omega}$ and $c = \frac{\Omega}{G}$. Now, we propose to use the following transformation:

$$\Gamma_\rho(\phi) = \exp\{-\frac{i}{c}[(v_t\tilde{k}_y - v_y\tilde{E})\phi - v_t\tilde{\xi}\sin\phi\sin\theta]\}\Phi_\rho(\phi). \tag{A3}$$

Then, we reduce the Eqs. (A1) and (A2) to the following form:

$$\frac{d\Gamma_A(\phi)}{d\phi} = iC^*(\phi)\Gamma_B(\phi), \tag{A4}$$

$$\frac{d\Gamma_B(\phi)}{d\phi} = iC(\phi)\Gamma_A(\phi), \tag{A5}$$

where $C(\phi) = [v_x(\tilde{k}_x - \tilde{\xi}\cos\phi\cos\theta) + iv_y(\tilde{k}_y - \tilde{\xi}\cos\phi\sin\theta)]/c$.

From Eqs. (A4) and (A5) we can obtain the following equations:

$$\frac{d^2\Gamma_A(\phi)}{d\phi^2} - \frac{1}{C^*(\phi)}\frac{dC^*(\phi)}{d\phi}\frac{d\Gamma_A(\phi)}{d\phi} + |C(\phi)|^2\Gamma_A(\phi) = 0, \tag{A6}$$

$$\frac{d^2\Gamma_B(\phi)}{d\phi^2} - \frac{1}{C(\phi)}\frac{dC(\phi)}{d\phi}\frac{d\Gamma_B(\phi)}{d\phi} + |C(\phi)|^2\Gamma_B(\phi) = 0. \tag{A7}$$

Inserting Eq. (A4) into Eq. (A6), and Eq. (A5) into Eq. (A7), we obtain that

$$\frac{d^2\Gamma_A(\phi)}{d\phi^2} - i\frac{dC^*(\phi)}{d\phi}\Gamma_B(\phi) + |C(\phi)|^2\Gamma_A(\phi) = 0, \tag{A8}$$

$$\frac{d^2\Gamma_B(\phi)}{d\phi^2} - i\frac{dC(\phi)}{d\phi}\Gamma_A(\phi) + |C(\phi)|^2\Gamma_B(\phi) = 0. \tag{A9}$$

And

$$\frac{dC(\phi)}{d\phi} = \tilde{\xi}\sin\phi[(v_x/c)\cos\theta + i(v_y/c)\sin\theta] = \Lambda\tilde{\xi}\sin\phi e^{i\beta},$$

where $\Lambda = (1/c)\sqrt{v_x^2\cos^2\theta + v_y^2\sin^2\theta}$ and $\beta = \arctan((v_y/v_x)\tan\theta)$.

We consider the transformation:

$$\Gamma_A(\phi) = e^{-i(\beta/2)}\chi_A(\phi), \tag{A10}$$

$$\Gamma_B(\phi) = e^{i(\beta/2)}\chi_B(\phi). \tag{A11}$$

Besides, if we consider that

$$\chi(\phi) = \begin{pmatrix}\chi_A(\phi)\\ \chi_B(\phi)\end{pmatrix}, \tag{A12}$$

then, we can reduce Eqs. (A8) and (A9) to the following equation:

$$\frac{d^2}{d\phi^2}\chi(\phi) + [|C(\phi)|^2 - i(\Lambda\tilde{\xi})\sigma_x\sin\phi]\chi(\phi) = 0. \tag{A13}$$

Now, observe that

$$\Lambda\tilde{\xi} = \frac{1}{\hbar\Omega}\zeta, \tag{A14}$$

where $\zeta = (eE_0/c\Omega)\sqrt{v_x^2\cos^2\theta + v_y^2\sin^2\theta}$, also

$$|C(\phi)|^2 = \left(\frac{1}{\hbar\Omega}\right)^2\left[\epsilon^2 + \zeta^2\cos^2\phi - 2\zeta\frac{\vec{v}\cdot\vec{\kappa}}{|\vec{v}|}\cos\phi\right], \tag{A15}$$

where $\epsilon = \hbar\sqrt{(v_xk_x)^2 + (v_yk_y)^2}$, $\vec{v} = (v_x\cos\theta, v_y\sin\theta)$ and $\vec{\kappa} = \hbar(v_xk_x, v_yk_y)$. Therefore, Eq. (A13) can be written as

$$\frac{d^2}{d\phi^2}\chi(\phi) + F(\phi)\chi(\phi) = 0, \tag{A16}$$

with $F(\phi)$ defined as

$$F(\phi) = \left(\frac{1}{\hbar\Omega}\right)^2\left[\zeta^2\cos^2\phi - 2\zeta\frac{\vec{v}\cdot\vec{\kappa}}{|\vec{v}|}\cos\phi\right] + \left(\frac{\epsilon}{\hbar\Omega}\right)^2 - i\frac{\zeta}{\hbar\Omega}\sigma_x\sin\phi. \tag{A17}$$

Remark: If we define $v_F = v_x = v_y$, $v_t = 0, \theta = 0$, then Eq. (A16) is reduced to the case of graphene as expected [28].

APPENDIX B

Let us estimate the gap size for a microwave of frequency $\Omega = 50$ GHz with an intensity $E_0 = 2$ V/m of the electric field. First, we calculate the value of q, given by

$$q(\theta) = -\left[\frac{\sqrt{(v_x^2\cos\theta)^2 + (v_y\sin\theta)^2}}{2\hbar\Omega}\left(\frac{eE_0}{c\Omega}\right)\right]^2. \tag{B1}$$

Thus, for $\theta = 0$, we have

$$q(0) = -0.2754, \tag{B2}$$

and for $\theta = \pi/2$, we obtain

$$q(\pi/2) = -0.1773. \tag{B3}$$

Thus, the gap of nth order is given by

$$\Delta_n(\theta) = \hbar\Omega\sqrt{|b_n(q) - a_n(q)|}. \tag{B4}$$

Finally, we evaluate $b_n(q)$ and $a_n(q)$ for the first-order gap:

$$\Delta_1(0) \approx 0.0243\times10^{-3}\text{eV}, \quad \Delta_1(\pi/2) \approx 0.0195\times10^{-3}\text{eV}. \tag{B5}$$

[1] K. S. Novoselov, A. K. Geim, S. V. Morozov, D. Jiang, Y. Zhang, S. V. Dubonos, I. V. Grigorieva, and A. A. Firsov, Electric field effect in atomically thin carbon films, Science **306**, 666 (2004).

[2] A. H. Castro Neto, F. Guinea, N. M. R. Peres, K. S. Novoselov, and A. K. Geim, The electronic properties of graphene, Rev. Mod. Phys. **81**, 109 (2009).

[3] S. Das Sarma, Shaffique Adam, E. H. Hwang, and E. Rossi, Electronic transport in two-dimensional graphene, Rev. Mod. Phys. **83**, 407 (2011).

[4] G. G. Naumis, S. Barraza-Lopez, M. Oliva-Leyva, and H. Terrones, Electronic and optical properties of strained graphene and other strained 2d materials: A review, Rep. Prog. Phys. **80**, 096501 (2017).

[5] J. Wang, S. Deng, Zhongfan Liu, and Zhirong Liu, The rare two-dimensional materials with Dirac cones, Natl. Sci. Rev. **2**, 22 (2015).

[6] T. O. Wehling, A. M. Black-Schaffer, and A. V. Balatsky, Dirac materials, Adv. Phys. **63**, 1 (2014).

[7] Z. Zhang, E. S. Penev, and B. I. Yakobson, Two-dimensional boron: structures, properties and applications, Chem. Soc. Rev. **46**, 6746 (2017).

[8] X.-F. Zhou, X. Dong, A. R. Oganov, Q. Zhu, Y. Tian, and Hui-Tian Wang, Semimetallic Two-Dimensional Boron Allotrope with Massless Dirac Fermions, Phys. Rev. Lett. **112**, 085502 (2014).

[9] A. J. Mannix, X.-F. Zhou, B. Kiraly, J. D. Wood, D. Alducin, B. D. Myers, Xiaolong Liu, B. L. Fisher, U. Santiago, J. R. Guest, M. J. Yacaman, A. Ponce, A. R. Oganov, M. C. Hersam, and N. P. Guisinger, Synthesis of borophenes: Anisotropic, two-dimensional boron polymorphs, Science **350**, 1513 (2015).

[10] Li-Chun Xu, A. Du, and L. Kou, Hydrogenated borophene as a stable two-dimensional Dirac material with an ultrahigh Fermi velocity, Phys. Chem. Chem. Phys. **18**, 27284 (2016).

[11] A. Lopez-Bezanilla and P. B. Littlewood, Electronic properties of 8-*Pmmn* borophene, Phys. Rev. B **93**, 241405(R) (2016).

[12] M. Nakhaee, S. A. Ketabi, and F. M. Peeters, Tight-binding model for borophene and borophane, Phys. Rev. B **97**, 125424 (2018).

[13] A. D. Zabolotskiy and Yu. E. Lozovik, Strain-induced pseudomagnetic field in the Dirac semimetal borophene, Phys. Rev. B **94**, 165403 (2016).

[14] V. M. Pereira and A. H. Castro Neto, Strain Engineering of Graphene's Electronic Structure, Phys. Rev. Lett. **103**, 046801 (2009).

[15] M. Oliva-Leyva and G. G. Naumis, Sound waves induce Volkov-like states, band structure and collimation effect in graphene, J. Phys.: Condens. Matter **28**, 025301 (2016).

[16] M. Oliva-Leyva and G. G. Naumis, Generalizing the Fermi velocity of strained graphene from uniform to nonuniform strain, Phys. Lett. A **379**, 2645 (2015).

[17] M. Oliva-Leyva and G. G. Naumis, Understanding electron behavior in strained graphene as a reciprocal space distortion, Phys. Rev. B **88**, 085430 (2013).

[18] P. Roman-Taboada and G. G. Naumis, Spectral butterfly and electronic localization in rippled-graphene nanoribbons: Mapping onto effective one-dimensional chains, Phys. Rev. B **92**, 035406 (2015).

[19] A. E. Champo, P. Roman-Taboada, and G. G. Naumis, Landauer-büttiker conductivity for spatially-dependent uniaxial strained armchair-terminated graphene nanoribbons, Phys. E (Amsterdam, Neth.) **102**, 123 (2018).

[20] M. Oliva-Leyva and G. G. Naumis, Effective Dirac Hamiltonian for anisotropic honeycomb lattices: Optical properties, Phys. Rev. B **93**, 035439 (2016).

[21] G. G. Naumis and P. Roman-Taboada, Mapping of strained graphene into one-dimensional Hamiltonians: Quasicrystals and modulated crystals, Phys. Rev. B **89**, 241404(R) (2014).

[22] K. Sadhukhan and A. Agarwal, Anisotropic plasmons, friedel oscillations, and screening in 8-*pmmn* borophene, Phys. Rev. B **96**, 035410 (2017).

[23] T. Nishine, A. Kobayashi, and Y. Suzumura, Tilted-cone induced cusps and nonmonotonic structures in dynamical polarization function of massless Dirac fermions, J. Phys. Soc. Jpn. **79**, 114715 (2010).

[24] S. Verma, A. Mawrie, and T. K. Ghosh, Effect of electron-hole asymmetry on optical conductivity in 8-*pmmn* borophene, Phys. Rev. B **96**, 155418 (2017).

[25] S. K. Firoz Islam and A. M. Jayannavar, Signature of tilted Dirac cones in Weiss oscillations of 8 − *pmmn* borophene, Phys. Rev. B **96**, 235405 (2017).

[26] S. H. Zhang and W. Yang, Oblique klein tunneling in 8 − *pmmn* borophene $p-n$ junctions, Phys. Rev. B **97**, 235440 (2018).

[27] F. J. López-Rodríguez and G. G. Naumis, Analytic solution for electrons and holes in graphene under electromagnetic waves: Gap appearance and nonlinear effects, Phys. Rev. B **78**, 201406(R) (2008).

[28] F. J. López-Rodríguez and G. G. Naumis, Graphene under perpendicular incidence of electromagnetic waves: Gaps and band structure, Philos. Mag. **90**, 2977 (2010).

[29] K. Kristinsson, O. V. Kibis, S. Morina, and I. A. Shelykh, Control of electronic transport in graphene by electromagnetic dressing, Sci. Rep. **6**, 20082 (2016)

[30] O. V. Kibis, Metal-insulator transition in graphene induced by circularly polarized photons, Phys. Rev. B **81**, 165433 (2010).

[31] O. V. Kibis, K. Dini, I. V. Iorsh, and I. A. Shelykh, All-optical band engineering of gapped Dirac materials, Phys. Rev. B **95**, 125401 (2017).

[32] Y. Zhou and M. W. Wu, Optical response of graphene under intense terahertz fields, Phys. Rev. B **83**, 245436 (2011).

[33] S. V. Syzranov, M. V. Fistul, and K. B. Efetov, Effect of radiation on transport in graphene, Phys. Rev. B **78**, 045407 (2008).

[34] Z. Gu, H. A. Fertig, D. P. Arovas, and A. Auerbach, Floquet Spectrum and Transport through an Irradiated Graphene Ribbon, Phys. Rev. Lett. **107**, 216601 (2011).

[35] A. Iurov, G. Gumbs, O. Roslyak, and D. Huang, Photon dressed electronic states in topological insulators: Tunneling and conductance, J. Phys.: Condens. Matter **25**, 135502 (2013).

[36] G. Usaj, P. M. Perez-Piskunow, L. E. F. Foa Torres, and C. A. Balseiro, Irradiated graphene as a tunable Floquet topological insulator, Phys. Rev. B **90**, 115423 (2014).

[37] P. Roman-Taboada and G. G. Naumis, Spectral butterfly, mixed Dirac-Schrödinger fermion behavior, and topological states in armchair uniaxial strained graphene, Phys. Rev. B **90**, 195435 (2014).

[38] P. Roman-Taboada and G. G. Naumis, Topological edge states on time-periodically strained armchair graphene nanoribbons, Phys. Rev. B **96**, 155435 (2017).

[39] P. Roman-Taboada and G. G. Naumis, Topological flat bands in time-periodically driven uniaxial strained graphene nanoribbons, Phys. Rev. B **95**, 115440 (2017).

[40] P. Roman-Taboada and G. G. Naumis, Topological phase-diagram of time-periodically rippled zigzag graphene nanoribbons, J. Phys. Commun. **1**, 055023 (2017).

[41] M. Mehboudi, K. Utt, H. Terrones, E. O. Harriss, A. A. P. SanJuan, and S. Barraza-Lopez, Strain and the optoelectronic properties of nonplanar phosphorene monolayers, Proc. Natl. Acad. Sci. U.S.A. **112**, 5888 (2015).

[42] R. Carrillo-Bastos and G. G. Naumis, Band gaps and wavefunctions of electrons coupled to pseudo electromagnetic waves in rippled graphene, Phys. Status Solidi RRL **12**, 1800072 (2018).

[43] N. W. McLachlan, *Theory and Application of Mathieu Functions* (Clarendon Press, Oxford, 1947).

[44] A. S. Davydov, *Théory du Solide* (Mir Publishers, Moscow, 1980).

[45] L. D. Landau, On the vibrations of the electronic plasma, Zh. Eksp. Teor. Fiz. **16**, 574 (1946) [J. Phys. (Moscow) **10**, 25 (1946)].